CrystEngComm

Dynamic Article Links

Cite this: *CrystEngComm*, 2012, **14**, 7607–7615

www.rsc.org/crystengcomm

PAPER

Weakly-coordinated stable platinum nanocrystals†

Dorothea Marquardt,[a] Juri Barthel,[b] Markus Braun,[a] Christian Ganter[a] and Christoph Janiak*[a]

Received 6th June 2012, Accepted 20th August 2012
DOI: 10.1039/c2ce25904d

Stable platinum nanocrystals with small diameters (1.0–2.3 nm), that are stable for a long time, with narrow size distributions were easily and reproducibly prepared without any additional stabilizers in glycol, glycerol, the ionic liquids (ILs) 1-n-butyl-3-methyl-imidazolium tetrafluoroborate [BMIm][BF_4] and *N*-butyl-*N*-trimethyl-ammonium bis(trifluoromethylsulfonyl)imide [N_{4111}][NTf_2] or diphenylmethane (CH_2Ph_2) by thermal, photolytic or microwave assisted decomposition of the organometallic precursor methylcyclopentadienyl-trimethylplatinum(IV), (MeCp)$PtMe_3$. Decomposition of the easily dispensible, air and moisture stable organometallic Pt(IV) precursor (MeCp)$PtMe_3$ leads to well defined, small, crystalline and longterm stable Pt-nanoparticle (Pt-NP) dispersions without any additional surface-capping ligands. The Pt-NP/IL dispersion was shown to be a highly active catalyst (TOF 96 000 h^{-1} at 0.0125 mol% Pt and quantitative conversion) for the biphasic hydrosilylation of phenylacetylene with triethylsilane, to the distal and proximal products triethyl(2- and1-phenylvinyl)silane.

Introduction

Platinum-based nanocrystals, including in the form of alloys and core-shell composite nanoparticles, are widely used in chemical syntheses, magnetic, catalytic, and biomedical applications and in energy conversion devices.[1,2] Many different reactions, *e.g.* oxidations,[3] oxygen reduction,[4,5] hydrogenation,[6,7] dehydrogenation, hydrosilylation[8–11] and C–C coupling reactions that are essential in industrial processes are catalyzed by Pt and its alloys.[12,13] Pt-based nanoparticles (Pt-NPs) are used as electro catalysts[4,5] on carbon or SiO_2 supports in electrode layers in almost all proton exchange membrane fuel cell devices.[1,13]

The catalytic potential and selectivities of nano catalysts depend on the sizes and shapes of the nanoparticles.[14–16] Metal alloy, core-shell and yolk-shell[17] nanoparticles can be prepared using colloid solution techniques[8,14] from metal salts or organometallic precursors with reducing agents at high temperatures, by photolysis or sonolysis.[12,18] Reaction conditions including temperature, concentration or gas pressure affect the resulting nanostructures.[13]

Classical platinum precursors can be chosen from hexachloroplatinic acid, H_2PtCl_6 potassium tetrachloroplatinate, K_2PtCl_4, platinum bis-dibenzylidene acetone, $Pt_2(dba)_3$,[6,19] platinum acetylacetonate, $Pt(acac)_2$ or platinum hexafluoroacetylacetonate, $Pt(hfa)_2$.[13] Reducing agents, capping ligands or surfactants for aqueous systems are borohydrides, hydrazine, dihydrogen, citrate and ascorbic acid. Polyols, diols or amines are used in organic solvents.[13]

Organometallic hydrocarbyl precursors are favored metal sources for chemical vapor deposition (CVD) processes growing thin films of metals[18,20,21] and also became important in metal nanoparticle chemistry. The advantage of hydrocarbyl precursors containing alkyl, allyl, olefin or cyclopentadienyl groups is the satisfactory thermal, photolytic or sonolytic decomposition to give bare metal atoms condensing in the reaction medium to nanoparticles with a contaminant-free surface.[18,22] This synthetic approach is notably capable for the syntheses of precious metal-nanoparticles.[18] For platinum films from CVD processes the following organometallic complexes are favored because of their volatility, thermal stabilities and clean decomposition routes: *cis*-$PtCl_2(CO)_2$ (**1**), (η^5-C_5H_5)PtMe(CO) (**2**) or $Pt(PF_3)_4$ (**3**), Pt-complexes containing allyl- and (di)olefin ligands (**4–6**), $CpPtMe_3$ and its air and moisture stable derivates (**7**).[21]

Room temperature ionic liquids (ILs) are known to stabilize metal nanoparticles without additional capping ligands. Agglomeration of particles is prevented by weakly-coordinating IL-anions and -cations forming protective shells surrounding the particles.[23–28] The IL appears to limit the diffusion and growth of nanoparticles so that small particles form.

Here we describe the decomposition of the precursor methylcyclopentadienyl-trimethylplatinum(IV), (MeCp)$PtMe_3$ for Pt-NP generation (Scheme 1). The easily accessible, storable, short-term air and moisture stable (MeCp)$PtMe_3$ complex was used as a precursor for CVD processes[21] with Pt metal deposition[29] and as a highly efficient organometallic photo-initiator for hydrosilylation.[10,11] We decomposed the precursor

[a]*Institut für Anorganische Chemie und Strukturchemie, Heinrich-Heine Universität Düsseldorf, Universitätsstraße 1, D-40225 Düsseldorf, Germany. E-mail: janiak@uni-duesseldorf.de; Fax: +49-(0)211-8112287*
[b]*Gemeinschaftslabor für Elektronenmikroskopie RWTH-Aachen, Ernst Ruska-Centrum für Mikroskopie und Spektroskopie mit Elektronen, D-52425, Jülich, Germany*

† Electronic supplementary information (ESI) available: ^{1}H-NMR spectra of the hydrosilylation reaction for entry 3 in Table 2. See DOI: 10.1039/c2ce25904d

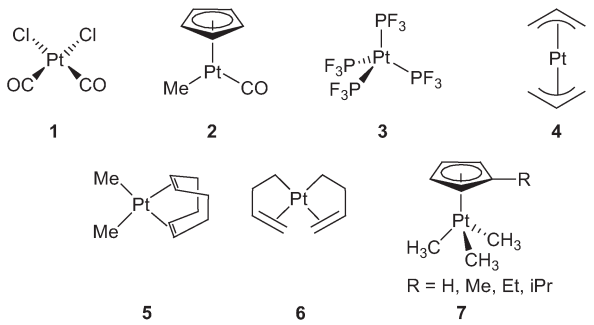

Scheme 1 Chemical structures of Pt precursors for CVD.

in glycol, glycerol, ionic liquids and diphenylmethane without any additional stabilizers (Scheme 2). Each of the chosen reaction media represent a different stabilizing principle, notably strong coordinating ligands in glycol and glycerol, weakly-coordinating anions and cations in ILs and phenyl-π-metal interactions[30] in diphenylmethane (CH_2Ph_2). In particular we focused on the synthesis of stable platinum nanocrystals in ionic liquids (Pt-NP/IL).

Results and discussion

The decomposition of the platinum hydrocarbyl complex (MeCp)$PtMe_3$ in different solvents with different stabilizing effects leads to dispersions of small and well defined Pt-NPs. For the desired Pt-NP dispersions of 0.5–2 mass% a defined amount of the complex (MeCp)$PtMe_3$ was suspended in the solvent under gentle warming (see Experimental section). Then, the Pt(IV) complex was decomposed by reduction to Pt(0) under microwave assisted heating, under conventional thermal treatment or under UV irradiation. The advantage of such hydrocarbyl precursors is their clean decomposition releasing volatile small organic fragments of the ligands which can be easily removed under reduced pressure. The decomposition in glycol, glycerol, ionic liquids and diphenylmethane reproducibly leads to small platinum nanoparticles of high crystallinity.

The decomposition of (MeCp)$PtMe_3$ can be initiated under photolytic and thermal conditions. Thermal decomposition by conventional heating was used for the solvent diphenylmethane with microwave-inactive molecules and for glycerol and glycol in comparison to microwave-assisted decomposition of the complex. Photolytic decomposition is a fast and energy-saving method, comparable to microwave-assisted heating. For microwave active solvents it is possible to provide fast and efficient thermal heating by microwave irradiation. Initially the microwaves

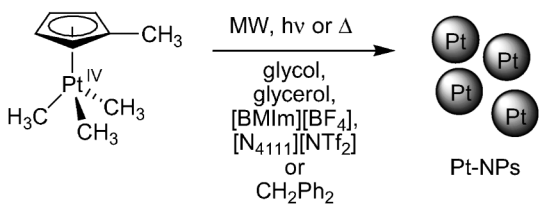

Scheme 2 Decomposition of (MeCp)$PtMe_3$ under different conditions (MW microwave irradiation; *hν* photolysis; Δ conventional thermal heating) and in different media.

are absorbed by the solvent molecules. Once metal particles have started to form, the microwaves will couple into these nucleation seeds to form hot spots where further decomposition and particle growth will occur. Thus, energy saving microwave irradiation accelerates the process of decomposition.[31] Microwave-assisted heating was successfully used for the microwave-active ionic liquids 1-n-butyl-3-methyl-imidazolium tetrafluoroborate [BMIm][BF_4] and *N*-butyl-*N*-trimethyl-ammonium bis(trifluoromethylsulfonyl)imide [N_{4111}][NTf_2]. For comparison UV decomposition of (MeCp)$PtMe_3$ was carried out in [BMIm][BF_4] and [N_{4111}][NTf_2].

Decomposition of (MeCp)$PtMe_3$ gave dispersions of nanocrystalline Pt-NPs with small average diameters that were stable for up to 11 months, typically between 1.0–2.3 nm in diameter and with narrow size distributions. Sizes depended somewhat on the dispersive medium glycol, glycerol, ionic liquids [BMIm][BF_4] and [N_{4111}][NTf_2] or diphenylmethane (CH_2Ph_2) and on the means of decomposition. The stability of the dispersions explicitly includes ligand-free Pt-NPs in ILs and in CH_2Ph_2.

Pt-NP dispersions were analyzed by high-resolution transmission electron microscopy (HRTEM) and high-angle annular dark-field-scanning transmission electron microscopy (HAADF-STEM). Particle diameters were determined from HAADF-STEM images. TEMs were carried out both on freshly prepared samples and on (the same) samples after several months. Particle sizes were measured from HAADF-STEM micrographs because this mode offers advantages over the HRTEM mode concerning the recognition of metal nanoparticles below 2 nm. The HAADF-STEM mode allows the identification of a higher number of particles. This leads to a smoother distribution of particle sizes displayed in a histogram to be approximately fitted by a Gaussian function.[32] Table 1 provides a listing of the diameters and their distributions of the obtained Pt-NPs according to solvent, method of decomposition and sample age.

Pt-NPs in glycol and glycerol

The analysis of a 0.5 mass% dispersion of Pt-NPs prepared from (MeCp)$PtMe_3$ in glycol or glycerol by conventional heating up to 150 °C–200 °C for 1.5 h reproducibly gave particle diameters between 0.3 and 3.6 nm with an average diameter of 1.7 ± 0.5 nm (Table 1, entry 1) in glycol (Fig. 1) and 1.5 ± 0.5 nm (Table 1, entry 4) in glycerol (Fig. 2) in an aged sample.

The microwave-assisted decomposition of the organometallic Pt precursor in glycol (Fig. 3) led to particle diameters of 2.3 ± 0.7 nm (Table 1, entry 2) for a freshly prepared sample and 1.7 ± 0.4 nm (Table 1, entry 2) for a 67 days old sample.

Photolytic decomposition of (MeCp)$PtMe_3$ led to stable nanoparticle dispersions of 0.5 mass% in glycol (Fig. 4) with an average particle diameter of 1.9 ± 0.7 nm (Table 1, entry 3). Resulting particle diameters were smaller in comparison to particles generated by microwave techniques (2.3 ± 0.7 nm). All three methods reliably afford Pt-NP dispersions of small diameters in glycol as a stabilizing solvent.

Pt-NPs in [BMIm][BF_4] and [N_{4111}][NTf_2]

Pt-NP dispersions in the ionic liquids [BMIm][BF_4] and [N_{4111}][NTf_2] were reproducibly synthesized by conventional heating, fast (minutes), hence, energy saving microwave-assisted

Table 1 Pt-NPs from $(MeCp)PtMe_3$ in different solvents and from different decomposition methods[a]

Entry	Solvent	Decomposition method[b]	Particle diameter and standard deviation σ/[nm] Fresh (1 day)	Older (57–331 days)
1	glycol	Δ	—	1.7 ± 0.6[c]
2	glycol	MW	2.3 ± 0.7[d]	1.7 ± 0.4[e]
3	glycol	*hv*	1.9 ± 0.7[f]	1.9 ± 0.6[g]
4	glycerol	Δ	—	1.5 ± 0.5[h]
5	[BMIm][BF_4]	Δ	3.9 ± 1.5[i]	—
6a	[BMIm][BF_4]	MW	—	1.5 ± 0.3 (57 days)[j]
6b	[BMIm][BF_4]	MW	—	1.5 ± 0.5 (228 days)[k]
7	[BMIm][BF_4]	*hv*	1.0 ± 0.3[l]	1.7 ± 0.1[m]
8	[N_{4111}][NTf_2][j]	Δ	1.4 ± 0.4[n]	—
9	[N_{4111}][NTf_2][j]	MW	1.4 ± 0.3[o]	—
10	[N_{4111}][NTf_2][j]	*hv*	1.1 ± 0.5[p]	1.2 ± 0.4[q]
11	CH_2Ph_2	Δ	—	1.6 ± 0.6[r]
12	CH_2Ph_2	*hv*	2.3 ± 0.7[s]	2.3 ± 0.6[t]

[a] Dispersion contained 0.5 mass% Pt unless noted otherwise. [b] Δ conventional thermal heating; MW microwave irradiation; *hv* photolysis. [c] 719 particles, sample age 122 days. [d] 257 particles. [e] 311 particles, sample age 67 days. [f] 86 particles. [g] 198 particles, sample age 67 days. [h] 648 particles, sample age 114 days. [i] 474 particles. [j] 505 particles, sample age 57 days. [k] 219 particles, sample age 228 days. [l] 194 particles. [m] 230 particles, sample age 67 day. [n] 310 particles. [o] 92 particles. [p] 2 mass% Pt 703 particles. [q] 824 particles, sample age 331 days. [r] 518 particles, sample age 57 days. [s] 412 particles. [t] 345 particles, sample age 67 days.

decomposition or by photolysis of $(MeCp)PtMe_3$. Complete decomposition was verified by ^{1}H-NMR spectroscopy through the absence of the characteristic signals from the Pt–Me groups of $(MeCp)PtMe_3$ (singlet at $\delta = 0.84$ ppm, flanked by Pt-satellites $J_{Pt,H} = 82$ Hz).[29]

The dispersions of Pt-NPs in ILs were stable over several months when kept under nitrogen atmosphere. The stability was verified by HAADF-STEM and HRTEM analysis for Pt-NPs in [BMIm][BF_4] and [N_{4111}][NTf_2] for samples of different ages synthesized by thermal decomposition (Table 1, entry 5; Fig. 5 and Table 1, entry 8; Fig. 6), microwave assisted decomposition (Table 1, entry 6a, 6b; Fig. 7 and 8 and Table 1, entry 9; Fig. 9) and photolytic decomposition (Table 1, entry 7; Fig. 10 and Table 1, entry 10; Fig. 11).

Thermal decomposition of the Pt(IV) precursor by conventionally heating in [BMIm][BF_4] led to a somewhat larger particle diameter distribution of 3.9 ± 1.5 nm (Table 1, entry 5, Fig. 5). In the IL [N_{4111}][NTf_2] thermal decomposition gave

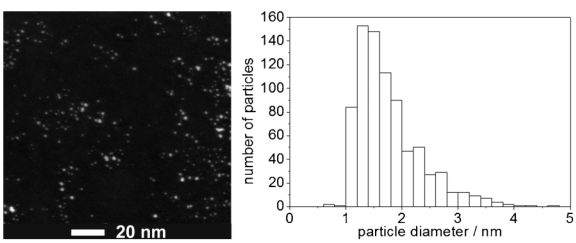

Fig. 1 Example of HAADF-STEM image of Pt-NPs prepared from $(MeCp)PtMe_3$ in glycol by thermal decomposition (Table 1, entry 1, 122 days old sample). Particle diameter distribution in histogram.

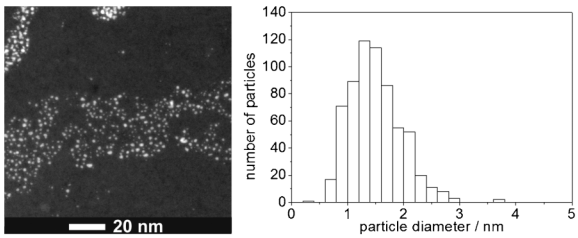

Fig. 2 Example of HAADF-STEM image of Pt-NPs prepared from $(MeCp)PtMe_3$ in glycerol under thermal decomposition (entry 4 in Table 1, 114 days old sample). Particle diameter distribution in histogram.

typical small particle diameters of 1.4 ± 0.4 nm (Table 1, entry 8, Fig. 6) similar to diameters from microwave or photolytic decomposition.

HRTEM images and HAADF-STEM images of Pt/[BMIm][BF_4] dispersions from microwave syntheses were taken from a Pt-NP dispersion 57 days after synthesis and the same sample was analyzed again by HAADF-STEM after 228 days (more than seven months) with no apparent change in particle diameter and distribution (Table 1, entries 6a and 6b; Fig. 8). The particle diameter distribution of the 57 days old sample was 1.5 ± 0.3 nm (0.8–5.1 nm) and the analysis of the same sample five months later gave very similar diameters from 0.8–5.1 nm with a distribution of 1.5 ± 0.5 nm. These results show that Pt-NP dispersions in the IL [BMIm][BF_4] were stable over several months without increase in average particle diameter or distributions.

The analysis of a freshly prepared Pt-NP/[N_{4111}][NTf_2] dispersion from microwave irradiation gave a particle diameter and distribution of 1.4 ± 0.3 nm (Table 1,entry 9, Fig. 9).

The decomposition of $(MeCp)PtMe_3$ under UV-irradiation was also carried out in ionic liquids. The resulting dispersions of Pt-NPs in [BMIm][BF_4] (0.5 mass%) and [N_{4111}][NTf_2] (2 mass%) were characterized by HAADF-STEM (Fig. 10 and 11).

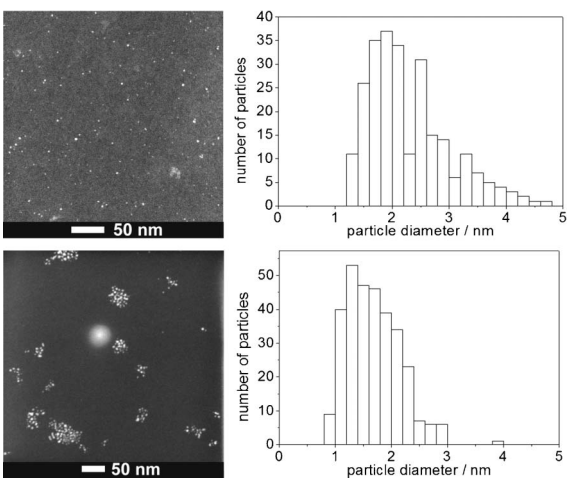

Fig. 3 Examples of HAADF-STEM images of Pt-NPs prepared from $(MeCp)PtMe_3$ in glycol under microwave-assisted decomposition (Table 1, entry 2) top: freshly prepared sample, bottom: older sample (67 days). Particle diameter distributions in histograms.

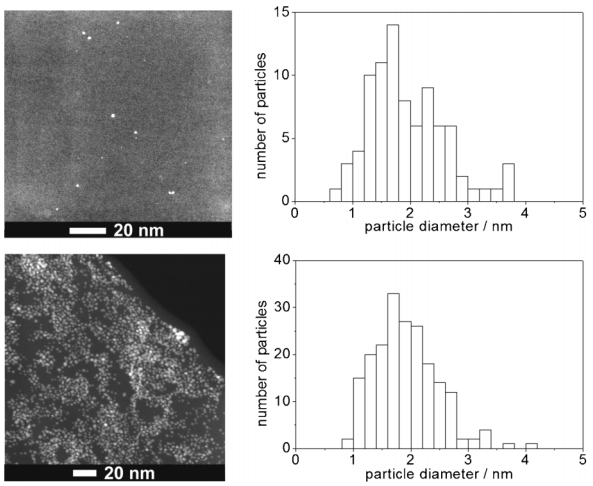

Fig. 4 Examples of HAADF-STEM images of Pt-NPs prepared from (MeCp)$PtMe_3$ in glycol by photolytic decomposition (Table 1, entry 3) top: freshly prepared sample; bottom: older sample (57 days). Particle diameter distributions in histograms.

Photolytic decomposition of (MeCp)$PtMe_3$ in ionic liquids led to very small Pt-NPs with diameter distributions of 1.0 $\pm$ 0.3 nm or 1.1 $\pm$ 0.5 nm for freshly prepared samples and 1.7 $\pm$ 0.1 nm or 1.2 $\pm$ 0.4 nm for aged samples (67 or 331 days) in [BMIm][BF_4] or [N_{4111}][NTf_2], respectively (Table 1, entry 7 or 10). Pt-NP dispersions in [N_{4111}][NTf_2] were very stable without a significant change of particle diameter distributions. Thus, the smallest and most homogenous dispersions of "ligand-free" Pt-NPs were prepared by photolytic decomposition of (MeCp)$PtMe_3$ in ionic liquids.

Platinum nanoparticles have also been prepared by hydrogen reduction (4 atm, 75 °C) of $Pt_2(dba)_3$ (dba = bis-dibenzylidene acetone) dispersed in the ionic liquids [BMIm][PF_6] or [BMIm][BF_4] with mean diameters of 2.3 nm or 3.4 nm, respectively.[6,7]

Pt-NPs in CH_2Ph_2

Pt-NPs prepared in CH_2Ph_2 by conventional heating up to 200 °C for 1.5 h gave particle diameters between 0.3 nm and 3 nm with an average of 1.6 $\pm$ 0.6 nm (Table 1, entry 11; Fig. 12).

The fast photolytic decomposition of (MeCp)$PtMe_3$ resulted in a 0.5 mass% Pt-NP dispersion in diphenylmethane within ten minutes. Particle diameters were determined from HAADF-STEM images to 2.3 $\pm$ 0.7 nm both for a freshly prepared and

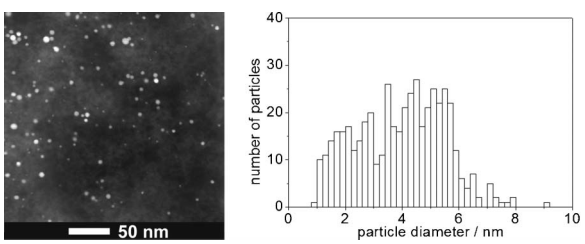

Fig. 5 HAADF-STEM image of Pt-NPs prepared from (MeCp)$PtMe_3$ in [BMIm][BF_4] by thermal decomposition (Table 1, entry 5, 1 day sample).

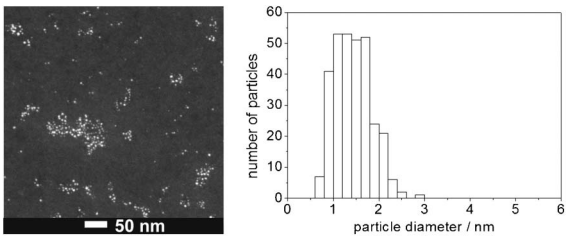

Fig. 6 HAADF-STEM image of Pt-NPs prepared from (MeCp)$PtMe_3$ in [N_{4111}][NTf_2] by thermal decomposition (Table 1, entry 8, 1 day sample).

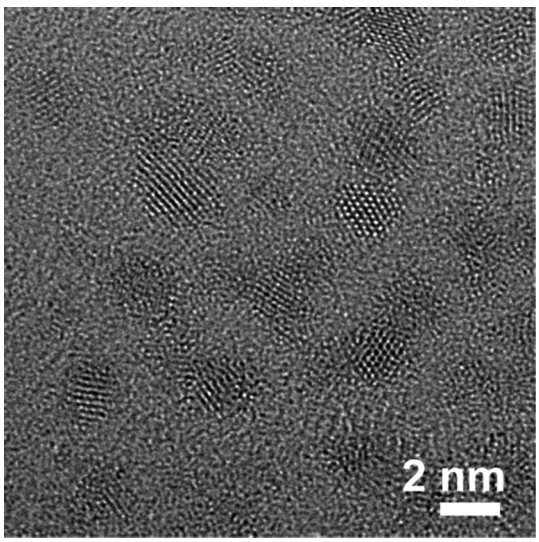

Fig. 7 HRTEM image of nanocrystalline Pt-NPs prepared from (MeCp)$PtMe_3$ in [BMIm][BF_4] by microwave irradiation (Table 1, entry 6a).

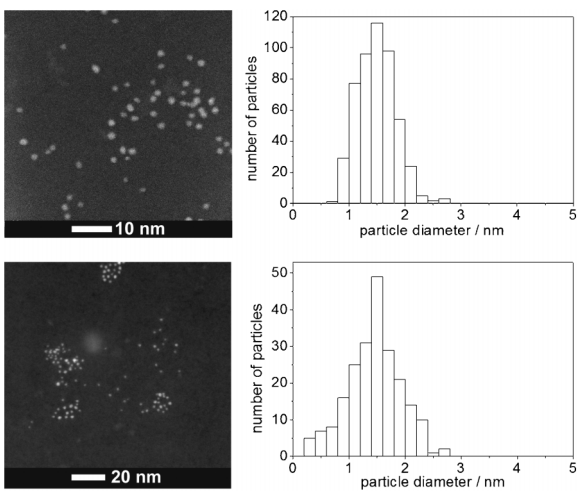

Fig. 8 HAADF-STEM images of Pt-NPs prepared from (MeCp)$PtMe_3$ in [BMIm][BF_4] under microwave-assisted decomposition. top: 57 days after synthesis (Table 1, entry 6a); bottom: 228 days after synthesis (Table 1, entry 6b). Particle diameter distribution in histogram.

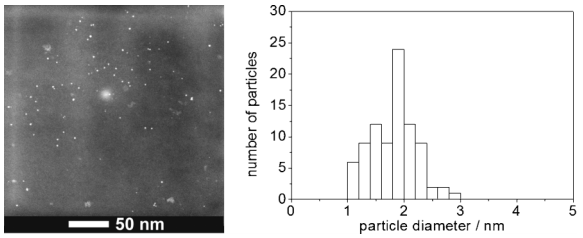

Fig. 9 HAADF-STEM image of Pt-NPs prepared from $(MeCp)PtMe_3$ in $[N_{4111}][NTf_2]$ under microwave assisted decomposition (entry 9 in Table 1, 1 day sample). Particle diameter distribution in histogram.

two-month aged sample (Table 1, entry 12; Fig. 13). Thus, the average diameter and its distribution did not change over a period of two months. These particle sizes are only slightly larger in comparison to Pt-NP sizes from photolytic decompositions in glycol and ionic liquids. Even though Pt-NPs were prepared in CH_2Ph_2 with slightly larger diameters, the stabilizing effect of CH_2Ph_2 seems to be very efficient. The stabilizing effect for Pt-NPs in diphenylmethane in the absence of conventionally coordinating ligands can be due to phenyl-π–Pt interactions between the phenyl ring and Pt surface atoms.[33]

Photolysis of related $CpPtMe_3$ in the presence of $HMe_2SiOSiMe_3$ in cyclohexane gave Pt-NPs between 1.0–2.5 nm.[11]

By comparison, the Pt-NP sizes obtained by different methods of decomposition from $(MeCp)PtMe_3$ in different solvents are very similar, in particular for the aged samples (Table 1). Noteworthy, Pt-NP dispersions in weakly-coordinating solvents such as non-functionalized ILs or diphenylmethane contain particles that are as small (namely around 1.5 nm) as in more coordinating solvents like glycol and glycerol. One may have expected that the stabilizing effect of coordinating ligands like glycol or glycerol with their hydroxy functionalities or even the supramolecular network of anions and cations in ILs would stabilize more efficiently than phenyl-π-metal interactions in

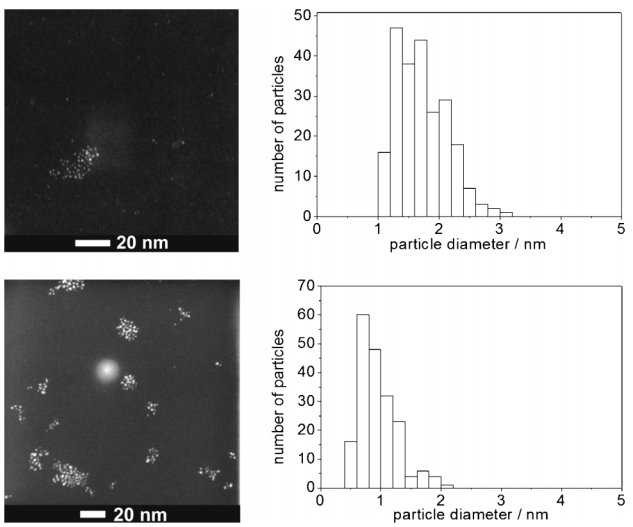

Fig. 10 HAADF-STEM images of Pt-NPs prepared by photolytic decomposition from $(MeCp)PtMe_3$ in $[BMIm][BF_4]$ (Table 1,entry 7); top: freshly prepared sample, bottom: older sample (67 days). Particle diameter distributions in histograms.

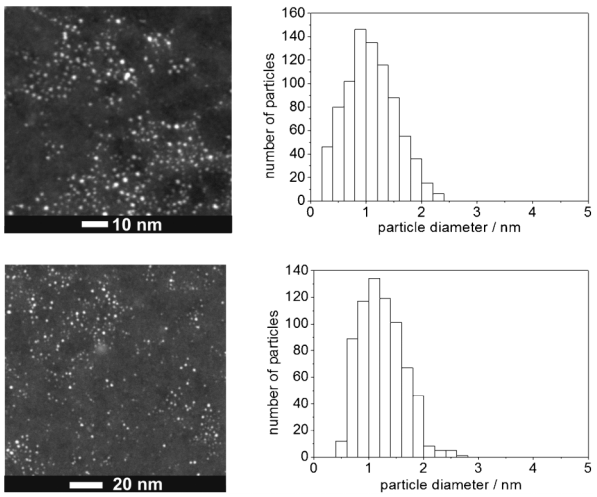

Fig. 11 HAADF-STEM images of Pt-NPs freshly prepared by photolytic decomposition from $(MeCp)PtMe_3$ in $[N_{4111}][NTf_2]$; top: freshly prepared sample; bottom: older sample (331 days) (Table 1, entry 10). Particle diameter distributions in histograms.

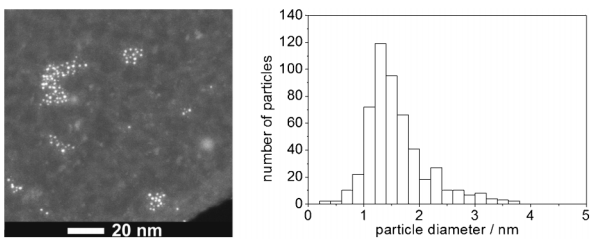

Fig. 12 Example of a HAADF-STEM image of Pt-NPs prepared in CH_2Ph_2 by conventional heating (150 °C) (Table 1, entry 11, 57 day old sample). Particle diameter distribution in histogram.

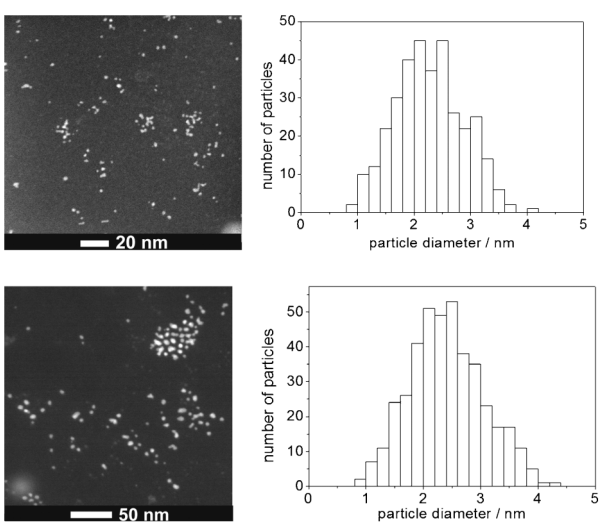

Fig. 13 Examples of HAADF-STEM images of Pt-NPs prepared in CH_2Ph_2 by photolytic decomposition from $(MeCp)PtMe_3$ (Table, entry 9); top: freshly prepared sample, bottom: 67 day old sample. Particle diameter distributions in histograms.

CH_2Ph_2. Yet, the diameter of Pt-NPs in CH_2Ph_2 is the same for an aged sample from conventional heating and only slightly larger for a fresh sample from photolysis. Thus, the stability of Pt-NP dispersions in weakly-coordinating solvents does not trail the stability in the stronger-coordinating media. The samples of Pt-NPs prepared in glycol, glycerol, ILs and diphenylmethane were analyzed by HAADF-STEM for up to eleven months (331 days) standing in their mother liquor at room temperature under nitrogen atmosphere and showed no significant differentiation in particle diameter and its distribution.

Crystallinity of the small Pt-NPs is evident from the HRTEM in Fig. 6 which clearly shows the lattice planes. Atom lattice parameters of nanocrystalline Pt-NPs were determined from Fourier power spectra of HRTEM image sections. This analysis gave an average value of interplanar d-spacing for each of the analyzed particles. The lattice parameters matched the theoretical value (0.39237 ± 3)[34] if $a = 0.392$ nm for the face-centered cubic (fcc) lattice of platinum metal. A detailed analysis of HRTEM image sections showed primarily particle orientations with the {110} and some with the {211} zone axis facing up (Fig. 14).

In this context we note a systematic investigation on the structure and stability of polyhedral Pt nanocrystals by atomistic simulations Pt nanocrystals, enclosed by high-index facets of {310}, {311}, and {331} are suggested to possess better stability and higher dangling bond density of surface compared with those ones with low-index facets, such as {111}, {100} and {110}. Octahedral nanocrystals with {111} facets, though they have excellent structural and thermal stabilities, present the lowest dangling bond density of the surface.[35]

In a recent study by Pelzer *et al.*, platinum nanoparticles 2 nm in diameter and containing *ca.* 200 atoms covered with n-octylsilyl groups were prepared. These Pt-NPs had a cubo octahedral shape with edges with a length of three atoms.[36]

Biphasic Pt-NP catalyzed hydrosilylation reactions

The Pt-NP/[BMIm][BF_4] dispersions were tested as catalysts for biphasic reactions of phenylacetylene with triethylsilane (Scheme 3, Table 2). A low solubility of the hydrosilylation starting materials and products with the IL led to the formation of two phases. This reaction mixture was chosen as a model system for the hydrosilylation of terminal acetylenes with alkylsilanes. The catalytic reaction was initially carried out under conventional heating in an oil bath. Performing the reaction under MW conditions was, however, a time and energy saving alternative to the conventional oil bath heating.

Conventional oil bath heating gave lower conversions at longer reaction times than the same reactions under microwave (MW) heating (compare entries 1 to 3 and 2 to 4 in Table 2). With MW heating quantitative conversion could be reached in a reaction time as short as 10 or even 5 min under similar conditions (entries 5 and 6 in Table 2). At the short reaction time of 5 min the temperature reached in the reaction mixture through MW heating critically depended on the amount of IL or Pt-NP/IL dispersion and varied from 150 °C to 90 °C (Table 2, entry 6–10). Phenylacetylene and triethylsilane are MW inactive. With a lower amount of MW-active IL (20 instead of 40 μL) or Pt-NPs (0.25 or 0.125 mass% instead of 0.5 mass% in IL) in the reaction

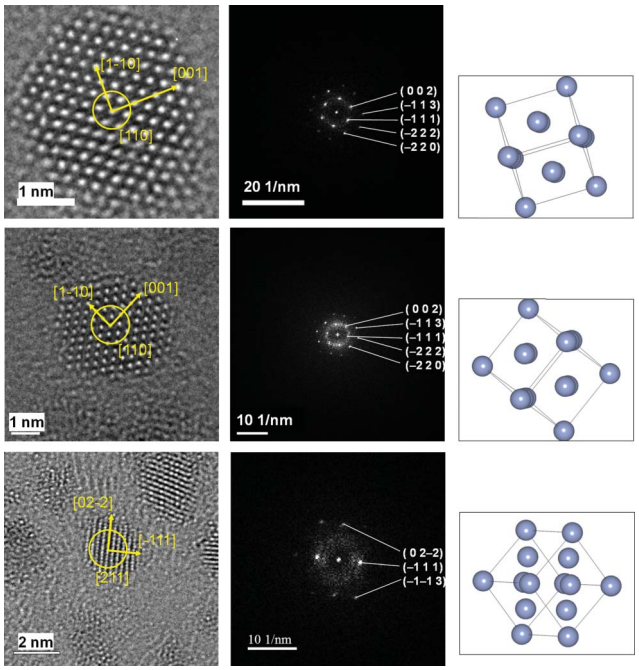

Fig. 14 Left: HRTEM image section, cut from original image of Pt-NPs prepared in [BMIm][BF_4] by MW irradiation (*cf.* Fig. 7). Middle: Digital Fourier power spectra from the cut image region. Right: Unit cell orientation.

mixture (entries 7–9) a temperature of only 90 °C was reached during 5 min MW irradiation and the conversion dropped to 35–38%. To reach quantitative conversion again at 0.125 mass% Pt in IL it was necessary to bring the amount of IL to 90 μL in order to reach the required reaction temperature of 150 °C within 5 min again (compare entry 9 and 10). This addition of IL lowered the Pt mass% in IL to 0.06 mass%. At these conditions a maximum turnover frequency (TOF) of 96 000 h^{-1} was achieved (entry 10).

During the hydrosilylation reaction the product mixture turned from the light yellow color of the substrate mixture to dark yellow or orange. In turn the dark brown Pt-NP/IL turned to light brown. These color changes of the reaction mixture could hint to Pt leaching from the IL to the product phase, but no traces of Pt-NP could be found in the product phase by HAADF-STEM. At the same time, after separating the product phase from the IL phase of the run in entry 10 and adding fresh substrate the conversion was negligible (3%, entry 11) and no reactivity was observed anymore when this procedure was repeated (entry 12). Thus, we suggest catalyst poisoning, *e.g.*, by *in situ* formed *N*-heterocyclic carbenes (NHCs) from the 1,4-alkyl substituted imidazolium cation of the ionic liquid. Those

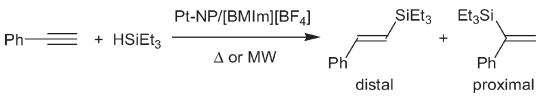

Scheme 3 Biphasic hydrosilylation of phenylacetylene with triethylsilane by Pt-NP dispersions in [BMIm][BF_4] to yield distal triethyl(styryl)silane [triethyl(2-phenylvinyl)silane] and proximal triethyl(1-phenylvinyl)silane.

Table 2 Biphasic hydrosilylation of phenylacetylene with triethylsilane, by Pt-NP dispersions in $[BMIm][BF_4]$[a]

Entry	Pt catalyst/ μmol	Molar ratio substrate : catalyst	Mass% Pt in IL	V(IL)/μl	Reaction time/min	Conversion[b]/%	TOF[c]/h^{-1}	Ratio[d] distal : proximal
1	1.25	4000 : 1	0.5	410	60, Δ	10	400	4 : 1
2	12.5	400 : 1	0.5	40	60, Δ	50	200	4 : 1
3	12.5	400 : 1	0.5	410	6	100	4000	4 : 1
4	1.25	4000 : 1	0.5	20	20	90	10 900	2 : 1
5	2.5	2000 : 1	0.5	40	10	100	11 800	2 : 1
6	2.5	2000 : 1	0.5	40	5	100	24 100	1.6 : 1
7	1.25	4000 : 1	0.5	20	5	38	18 300	3.3 : 1
8	1.25	4000 : 1	0.25	40	5	35	16 900	2.6 : 1
9	0.625	8000 : 1	0.125	40	5	36	34 700	2 : 1
10	0.625	8000 : 1	0.06	90	5	100	96 000	1.4 : 1
11[e]	0.625	8000 : 1	0.06	90	5	3	2900	4 : 1
12[e]	0.625	8000 : 1	0.06	90	5	no reaction	—	—

[a] Phenylacetylene (0.54 ml, 5.0 mmol) and triethylsilane (0.79 ml, 5.0 mmol). Microwave (MW) heating, except for entries 1 and 2 with thermal heating (Δ). The pressure inside the MW reactor was set to p_{max} = 3.0 bar. The applied MW energy depended on the pressure and so the reaction temperature varied from 90 °C–150 °C. The maximum reaction temperature was set to 150 °C. It was observed that the reaction temperature which could be reached depended on the amount of IL or Pt-NPs in the biphasic reaction mixture. [b] Conversion determined from crude products by ^{1}H-NMR spectroscopy. [c] TOF = turnover frequency [mol(product)/mol(Pt) × h^{-1}]. [d] Determined from ^{1}H-NMR spectra of the reaction mixture. See example spectrum for entry 3 as Fig. S1 in ESI.† ^{1}H-NMR signals for the mixture of distal (main product) and proximal (byproduct) products were taken from the literature.37 [e] Entry 11 and 12 are the second and third run, respectively, of entry 10 after separating the substrate phase from the IL phase and adding fresh substrate.

NHCs are known as strong ligands coordinating to single transition-metal centers.[38,39]

Distillation of the product phase from the Pt-NP/IL dispersion inhibited catalyst activity completely. A second run gave no conversion.

Particle aggregation can be ruled out as a reason for deactivation. HAADF-STEM analysis of the product mixtures from two catalytic runs still showed Pt-NPs with unchanged average diameters of about 1.5 nm and small distribution of ±0.4 nm (Fig. 15 and 16).

Experimental

Methylcyclopentadienyl-dimer was received from Alfa Aeser, n-butyllithium (1.6 mol L^{-1} in hexane), methyllithium (1.6 mol L^{-1} in diethyl ether), diphenylmethane 99%, anhydrous glycerol, 99.5%, 1,2-dibromoethane 98%, potassium hexachloroplatinate(IV) 98% and glycol 99.5% from Sigma Aldrich, potassium iodide 99.5% from Merck, ionic liquids 1-n-butyl-3-methyl-imidazolium tetrafluoroborate $[BMIm][BF_4]$ and tri-n-butyl-methyl-ammonium bis(trifluoromethylsulfonyl)imide $[N_{4111}][NTf_2]$ were purchased from IoLiTec. The ILs were dried and degassed in vacuum (1 h, 85 °C oil bath temperature).

$(MeCp)PtMe_3$ was obtained through the reaction of MeCpLi with $(Me_3PtI)_4$.[40,41]

Synthesis of trimethylplatinum(IV)-iodide tetramer, $(Me_3PtI)_4$

Potassium hexachloroplatinate(IV) (4.00 g, 8.23 mmol) was dispersed in THF (8 mL) and the yellow dispersion was cooled to 0 °C. Methyllithium (4.8 mL, 7.72 mmol) was added in 2 ml steps over a period of 4 h at 0 °C. The cooling bath was removed and the yellow–brown dispersion was slowly warmed to room temperature. The resulting white slurry was again cooled to 0 °C and 1,2-dibromoethane (3.68 mL, 42.8 mmol) was added over a period of 60 min. For quenching an aqueous solution of hydrochloric acid (c = 2 mol L^{-1}, 1 ml), saturated with potassium iodide was added dropwise to the reaction mixture. The ether and aqueous phase was separated. The aqueous phase was extracted twice with diethyl ether. The combined organic phases were washed with brine and dried over Na_2SO_4. The organic solvent was removed under reduced pressure and the dark red colored crude product was washed with acetone. A light-brown solid was obtained in 90% yield.

^{1}H-NMR (200 MHz, $CDCl_3$): δ (ppm) = 1.73 (s, $^2J_{Pt-H}$ = 77 Hz). ^{13}C–NMR (126 MHz, $CDCl_3$): δ (ppm) = 13.2 (s, $^1J_{Pt-C}$ = 686 Hz).

Synthesis of (η^5-methylcyclopentadienyl)trimethylplatinum(IV)

Methylcyclopentadienyl-dimer was cracked to the monomers by distillation (180 °C oil bath temperature) and stored at −20 °C in the dark. Methylcyclopentadiene monomer (0.64 g, 7.99 mmol) was dissolved in THF (8 mL) and cooled to −78 °C. *n*-Butyllithium (4.5 mL, 7.20 mmol) was added dropwise, keeping the temperature at −78 °C. Then the cooling bath was removed and the reaction mixture slowly warmed to room temperature under continuous stirring. A yellow precipitate formed. THF was added to resolve the solid and a light-yellow solution was formed. This MeCpLi solution was added to a dispersion of $(Me_3PtI)_4$ (2.36 g, 6.43 mmol) in THF (15 ml) and the mixture stirred for 60 min at RT. Water (20 ml) was added and the organic and aqueous phase separated. The aqueous

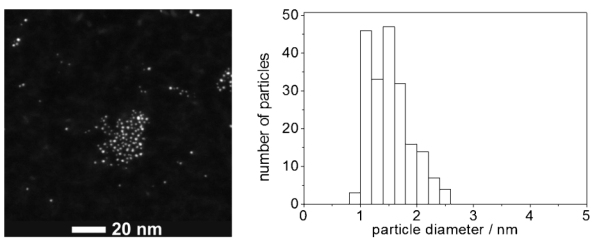

Fig. 15 HAADF-STEM example image of Pt-NPs in the product mixture after hydrosilylation catalysis: Pt-NPs after catalysis according to entry 1 in Table 2 (particle diameter 1.5 ± 0.4 nm from analysis of 194 particles). Particle diameter distribution in histogram.

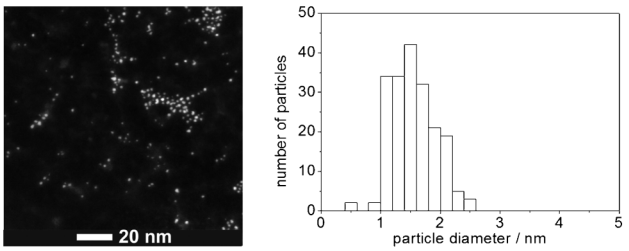

Fig. 16 HAADF-STEM example images of Pt-NPs in the product mixture after hydrosilylation catalysis: Pt-NPs after catalysis according to entry 2 in Table 2 (particle diameter 1.6 ± 0.4 nm from analysis of 202 particles. Particle diameter distribution in histogram.

phase was extracted with hexane and the combined organic phases were washed with brine and dried over Na_2SO_4. The organic solvent was removed under reduced pressure. The crude product was purified by sublimation (25 °C, 2 mbar) to give a light-yellow solid (yield 94%).

^{1}H-NMR (200 MHz, $CDCl_3$): δ (ppm) = 5.55–5.50 (m, 2H, Cp–H–α), 5.29–5.23 (m, 2H, Cp–H–β), 1.96 (s, 3H, $^3J_{Pt-H}$ = 6 Hz, Cp–CH_3), 0.84 (s, 9H, $^2J_{Pt-H}$ = 82 Hz, Pt–CH_3). ^{13}C–NMR (126 MHz, $CDCl_3$): δ (ppm) = 114.61 (s, $^1J_{Pt-C}$ = 14 Hz, Cp–C-*ipso*), 95.91 (s, $^1J_{Pt-C}$ = 4 Hz, Cp–C–α), 91.68 (s, $^1J_{Pt-C}$ = 6 Hz, Cp–C–β), 11.85 (s, Cp–CH_3), –18.37 (s, $^1J_{Pt-C}$ = 716 Hz, Pt–CH_3).

Instrumentation

Photolysis: Laboratory UV reactor system (150 W Hg-UV immersion lamp TQ 150, λ_{max} = 254 nm, Heraeus GmbH, Hanau).

Laboratory microwave system: CEM Discover microwave reactor.

^{1}H-NMR: Bruker Avance DRX 200 spectrometer.

^{13}C-NMR: Bruker Avance DRX 500 spectrometer.

High resolution transmission electron microscopy (HRTEM)

HRTEM micrographs were taken from a FEI TITAN 80–300 image CS-corrected operating at 300 kV. High-angle annular dark-field-scanning transmission electron microscopy (HAADF-STEM) pictures were taken from FEI TECNAI G^2 F 20 HR(S)TEM and FEI TITAN 80–300 probe CS-corrected HRSTEM.

Particle diameters were measured from HAADF-STEM micrographs and histograms with diameter distributions were prepared there from. All samples for HRTEM/HAADF-STEM were prepared by dropping a small amount of Pt-NP/solvent dispersion on a carbon coated copper grid lying on filter paper. Excess dispersion was removed by covering the grid with filter paper. After lying for a few minutes, the grid was washed with acetone (for IL and diphenylmethane) or ethanol (for glycol and glycerol) and it was plasma cleaned (10 s) to avoid contamination by decomposition of organic compounds during microscopy.

Pt-NP synthesis-typical protocol

Pt-NP dispersions with 0.5 or 2 mass% Pt (relative to solvent) were prepared by suspending the required amount of (MeCp)$PtMe_3$ (Table 3) under gentle warming in glycol, glycerol, [BMIm][BF_4], [N_{4111}][NTf_2] or diphenylmethane. The decomposition reaction was carried out either under conventional thermal heating for 1.5 h in an oil bath at 150 °C (glycol) or 200 °C (glycerol, CH_2Ph_2); under photolysis (λ_{max} = 254 nm, 10 min) or under microwave irradiation (20 W, 0.5 min run time, 5.5 min hold time). The gaseous byproducts were removed under reduced pressure.

Hydrosilylation reactions

All reactions by thermal or microwave-assisted heating were carried out using Schlenk-techniques under inert nitrogen atmosphere in dried Schlenk-tubes. For the microwave-assisted heating microwave vials with a Teflon septum were used. These vials were charged with starting materials and catalysts having the vial in a Schlenk tube under inert gas.

In a typical procedure, phenylacetylene (0.54 ml, 5.0 mmol) and triethylsilane (0.79 ml, 5.0 mmol) were put in the reaction vessel and then the required amount of Pt-NP/IL dispersion (mostly 0.5 mass% Pt) (0.625–12.5 μmol Pt, see Table 2) was added and a two-phase system was formed with a slightly yellow upper substrate phase and a dark brown lower Pt/IL phase.

The reaction mixture was heated in an oil bath for 1 h at 90 °C (oil bath temperature) (Table 2, entry 1–2) or by using a microwave procedure (200 W, p_{max} was set to 3.0 bar, t_{max} was set to 250 °C), reaction time, see Table 2, entries 3–12).

After cooling the reaction mixture to room temperature and after phase separation an aliquot of the crude product phase was assessed for conversion by ^{1}H-NMR spectroscopy (Table 2, entry 1–12).

The Pt-NP/IL catalyst was recovered by pipetting the product phase out of the reaction vessel. To test the activity of the recovered catalyst (Table 2 entry 11–12), the catalyst phase was re-charged with phenylacetylene (0.54 ml, 5.0 mmol) and triethylsilane (0.79 ml, 5.0 mmol) as above.

Table 3 Amount of (MeCp)$PtMe_3$[a] for the preparation of Pt-NP colloids in different solvents

Solvent	m (solvent)/g (V = 1 ml)	m (MeCp)$PtMe_3$/mg		n (MeCp)$PtMe_3$/mmol	
		for 0.5 mass% Pt	for 2 mass% Pt	for 0.5 mass% Pt	for 2 mass% Pt
glycol	1.1	8.4	—	0.026	—
glycerol	1.2	9.5	—	0.030	—
[BMIm][BF_4]	1.2	9.4	37.6	0.029	0.118
[N_{4111}][NTf_2]	1.4	10.9	43.3	0.034	0.136
CH_2Ph_2	1.0	7.9	—	0.025	—

[a] molar mass of (MeCp)$PtMe_3$ = 319.31 g mol^{-1}; 61.1 mass% Pt in (MeCp)$PtMe_3$.

Conclusions

Platinum nanocrystals could reproducibly be prepared from(MeCp)$PtMe_3$ under conventional thermal heating, photolysis or microwave irradiation in coordinating (glycol, glycerol) or non-coordinating solvents (non-functionalized ILs, diphenylmethane). Pt-NPs were highly crystalline (from HRTEM), of small diameters (typically between 1.0–2.3 nm) and narrow diameter distribution ($\pm$0.7 nm). There was no clear dependence of the Pt-NP size and size distribution on the solvent or method of preparation. It is noteworthy that all of these Pt-NP dispersions were stable for several months without any sign of aggregation. The Pt-NP/IL dispersion was verified as a highly active catalyst for the biphasic hydrosilylation of phenylacetylene with triethylsilane, to the distal and proximal products triethyl(2- and 1-phenylvinyl)silane.

Acknowledgements

Financial support through the DFG grant Ja466/17-1 is gratefully acknowledged.

References

1 Y. Liu, D. Li and S. Sun, *J. Mater. Chem.*, 2011, **21**, 12579–12587.
2 S.-H. Chang, M.-H. Yeh, C.-J. Pan, K.-J. Chen, H. Ishii, D.-G. Lui, J.-F. Lee, C.-C. Lui, J. Rick, M.-Y. Cheng and B.-J. Hwang, *Chem. Commun.*, 2011, **47**, 3864–3866.
3 N. Dimitratos, J. A. Lopez-Sanchez and G. J. Hutchings, *Chem. Sci.*, 2012, **3**, 20–44.
4 Z.-Y. Zhou, X. Kang, Y. Song and S. Chen, *Chem. Commun.*, 2012, **48**, 3391–3393.
5 R. Loukrakpam, P. Chang, J. Luo, B. Fang, D. Mott, I.-T. Bae, H. R. Naslund, M. H. Engelhard and C.-J. Zhong, *Chem. Commun.*, 2010, **46**, 7184–7186.
6 C. W. Scheeren, G. Machado, J. Dupont, P. F. P. Fichtner and S. R. Texeira, *Inorg. Chem.*, 2003, **42**, 4738–4742.
7 C. W. Scheeren, G. Machado, S. R. Teixeira, J. Morais, J. B. Domingos and J. Dupont, *J. Phys. Chem. B*, 2006, **110**, 13011–13020.
8 D. Troegel and J. Stohrer, *Coord. Chem. Rev.*, 2011, **255**, 1440–1450.
9 F. Alonso, R. Buitrago, Y. Moglie, J. Ruiz-Martínez, A. Sepúlveda-Escribano and M. Yus, *J. Organomet. Chem.*, 2011, **696**, 368–372.
10 V. Jakubek and A. J. Lees, *Inorg. Chem.*, 2004, **43**, 6869–6871.
11 L. D. Boardman, *Organometallics*, 1992, **11**, 4194–4201.
12 V. I. Pârvulescu and C. Hardacre, *Chem. Rev.*, 2007, **107**, 2615–2665.
13 Z. Peng and H. Yang, *Nano Today*, 2009, **4**, 143–164.
14 A. Fihri, M. Bouhrara, B. Nekoueishahraki, J.-M. Basset and V. Polshettiwar, *Chem. Soc. Rev.*, 2011, **40**, 5181–5203.
15 Y. Li, Q. Liu and W. Shen, *Dalton Trans.*, 2011, **40**, 5811–5826.
16 K. An, S. Alayoglu, T. Ewers and G. A. Somorjai, *J. Colloid Interface Sci.*, 2012, **373**, 1–13.
17 J. Liu, S. Z. Qiao, J. S. Chen, X. W. Lou, X. Xing and G. Q. Lu, *Chem. Commun.*, 2011, **47**, 12578–12591.
18 (*a*) T. Gutel, J. Garcia-Antõn, K. Pelzer, K. Philippot, C. C. Santini, Y. Chauvin, B. Chaudret and J.-M. Basset, *J. Mater. Chem.*, 2007, **17**, 3290–3292; (*b*) B. Chaudret and K. Phillipot, *Oil Gas Sci. Technol.*, 2007, **62**, 799–817; (*c*) D. Ciuculescu, F. Dumestre, M. Comensaña-Hermo and B. Chaudret, *Chem. Mater.*, 2009, **21**, 3987–3995; (*d*) T. Gutel, C. C. Santini, K. Philippot, A. Padua, K. Pelzer, B. Chaudret, Y. Chauvin and J.-M. Basset, *J. Mater. Chem.*, 2009, **19**, 3624–3631; (*e*) N. Atamena, D. Ciuculescu, G. Alcaraz, A. Smekhova, F. Wilhelm, A Rogalev, B. Chaudret, P. Lecante, R. E. Benfield and C. Amiens, *Chem. Commun.*, 2010, **46**, 2453–2455; (*f*) V. Latour, A. Maisonnat, Y. Coppel, V. Collière, P. Fau and B. Chaudret, *Chem. Commun.*, 2010, **46**, 2683–2685; (*g*) M. Zahmakiran, M. Tristany, K. Phillippot, K. Fajerwerg, S. Özkar and B. Chaudret, *Chem. Commun.*, 2010, **46**, 2938–2940; (*h*) C. Desvaux, P. Lecante, M. Respaud and B. Chaudret, *J. Mater. Chem.*, 2010, **20**, 103–109; (*i*) P. S. Campbell, C. C. Santini, D. Bouchu, B. Fenet, K. Philippot, B. Chaudret, A. A. H. Pádua and Y. Chauvin, *Phys. Chem. Chem. Phys.*, 2010, **12**, 4217–4223.
19 M. Tristany, M. Moreno-Mañas, R. Rosa Pleixat, B. Chaudret, K. Phillippot, Y. Guari, V. Matsura and P. Lecante, *New J. Chem.*, 2009, **33**, 1529–1534.
20 X.-M. Yan, C. Kim and J. M. White, *Thin Solid Films*, 2001, **391**, 62–68.
21 C. Thurier and P. Doppelt, *Coord. Chem. Rev.*, 2008, **252**, 155–169.
22 C. Pagès, Y. Coppel, M. L. Kahn, A. Maissonat and B. Chaudret, *ChemPhysChem*, 2009, **10**, 2234–2344.
23 J. Dupont and J. D. Jackson, *Chem. Soc. Rev.*, 2010, **39**, 1780–1804.
24 C. Vollmer and C. Janiak, *Coord. Chem. Rev.*, 2011, **255**, 2039–2057.
25 E. Redel, R. Thomann and C. Janiak, *Inorg. Chem.*, 2008, **47**, 14–16.
26 D. Marquardt, X. Xie, A. Taubert, R. Thomann and C. Janiak, *Dalton Trans.*, 2011, **40**, 8290–8293.
27 (*a*) S. F. L. Mertens, C. Vollmer, A. Held, M. H. Aguirre, M. Walter, C. Janiak and T. Wandlowski, *Angew. Chem., Int. Ed.*, 2011, **50**, 9735–9738; (*b*) C. Vollmer, E. Redel, K. Abu-Shandi, R. Thomann, H. Manyar, C. Hardacre and C. Janiak, *Chem.–Eur. J.*, 2010, **16**, 3849–3858; (*c*) E. Redel, M. Walter, R. Thomann, L. Hussein, M. Krüger and C. Janiak, *Chem. Commun.*, 2010, **46**, 1159–1161; (*d*) E. Redel, M. Walter, R. Thomann, C. Vollmer, L. Hussein, H. Scherer, M. Krüger and C. Janiak, *Chem.–Eur. J.*, 2009, **15**, 10047–10059; (*e*) E. Redel, J. Krämer, R. Thomann and C. Janiak, *J. Organomet. Chem.*, 2009, **694**, 1069–1075; (*f*) J. Krämer, E. Redel, R. Thomann and C. Janiak, *Organometallics*, 2008, **27**, 1976–1978; (*g*) E. Redel, R. Thomann and C. Janiak, *Chem. Commun.*, 2008, 1789–1791.
28 (*a*) F. Endres, *Angew. Chem., Int. Ed.*, 2003, **42**, 3428–3430; (*b*) F. Endres and S. Z. El Abedin, *Phys. Chem. Chem. Phys.*, 2006, **8**, 2101–2116.
29 Z. Xue, M. J. Strouse, D. K. Shuh, C. B. Knobler, H. D. Kaesz, R. F. Hicks and R. S. Williams, *J. Am. Chem. Soc.*, 1989, **111**, 8779–8784.
30 I. Favier, S. Massou, E. Teumaö, K. Philippot, B. Chaudret and M. Gómez, *Chem. Commun.*, 2008, 3296–3298.
31 C. Leonellia and T. J. Mason, *Chem. Eng. Process.*, 2010, **49**, 885–900.
32 B. Zhang, W. Zhang and D. S. Shu, *Microscopy and Analysis*, 2012, **26**, 15–20.
33 W. Chen, N. B. Zuckermann, X. Kang, D. Gosh, J. Konopelski and S. Chen, *J. Phys. Chem. C*, 2010, **114**, 18146–18152.
34 *Crystal Data Determinative Tables*, 3rd ed., **Vol. 2**, (J. D: Donnay, H. M. Ondik, ed.) 1973.
35 R. Huang, Y.-H. Wen, Z.-Z. Zhu and S.-G. Sun, *J. Mater. Chem.*, 2011, **21**, 11578–11584.
36 K. Pelzer, M. Havecker, M. Boualleg, J. P. Candy and J. M. Basset, *Angew. Chem., Int. Ed.*, 2011, **50**, 5170.
37 L. Yong, K. Kirleis and H. Butenschön, *Adv. Synth. Catal.*, 2006, **348**, 833–836.
38 L. Starkey, S. Campbell, K. R. Seddon and R. G. Finke, *Inorg. Chem.*, 2007, **46**, 10335–10344.
39 T. J. Geldbach, D. Zhao, N. C. Castillo, G. Laurenczy, B. Weyershausen and P. J. Dyson, *J. Am. Chem. Soc.*, 2006, **128**, 9773–9780.
40 US patent 2004/0010158 A1, S. H. Meiere and C. A. Hoover, Methods for producing organometallic compounds, 15 January 2004. Praxier Technology, Inc., Danbury, CT (USA).
41 US patent 6,809,212 B2, S. H. Meiere and C. A. Hoover, Methods for producing organometallic compounds, 26 October 2006, Praxier Technology, Inc., Danbury, CT (USA).